nature water

Article

https://doi.org/10.1038/s44221-025-00549-x

Headwater streams control the non-perennial fraction of the global river network

Received: 8 May 2025

Accepted: 28 October 2025

Published online: 06 January 2026

Check for updates

Gianluca Botter ✉, Francesca Barone & Nicola Durighetto

Quantifying the fraction of a river network that does not flow year-round is crucial, as the wetting and drying of channels governs important hydrological and biogeochemical services of watersheds. However, this remains challenging due to limited experimental data and the difficulty of accurately representing the total length of rivers draining a landscape. Here we present new global estimates of non-perennial stream fractions by extrapolating low-resolution global simulations and detailed field observations from experimental sites spanning diverse climatic settings. Our findings show that non-perennial streams are far more prevalent than previously recognized, both regionally and globally. When small headwater streams are comprehensively accounted for, the global fraction of non-perennial channels rises above 0.7 (up to 0.78), with regional estimates in relatively humid regions such as Italy and the eastern USA exceeding 0.5. The study reveals that, owing to the abundance of small upland streams, the effect of channel wetting and drying in headwaters persists even in much larger basins. The systematic prevalence of non-perennial streams across different watershed sizes calls for a paradigm shift in water science, emphasizing the importance of adequately considering channel network dynamics in the assessment of hydrological, ecological and societal services provided by rivers.

River networks are often perceived as static entities[1], yet streams continuously adjust their length and shape, expanding and contracting in response to the fluctuating hydrological conditions of the surrounding landscape[2–4]. Stream network dynamics represent a ubiquitous phenomenon across diverse climatic and geographic settings, from humid regions to arid landscapes[5–8]. When smaller, non-perennial streams—those that periodically cease to flow and/or become dry—are fully accounted for, the river network appears much denser than anticipated[9]. This makes an accurate definition of the extent of the channel domain a challenging task. Yet, experimental data and geomorphological analyses consistently show that the contributing area at the channel heads is rather small[10] (that is, $\ll 1\ \mathrm{km}^2$), which places the actual drainage density of river basins within the range of 1–100 km km^{-2} (ref. 11). While it is not possible to derive an exact value for the total length of the global river network, we attempted an estimate of the average global drainage density D_d by compiling a dataset of 344 empirical values reported in the literature[3,12–19]. Despite the presence of several upper outliers, the interquartile range of D_d remains relatively narrow (6.71 km km^{-2}), and the sample mean exceeds 10 km km^{-2} (that is, 10.48 ± 1.13 km km^{-2}; Methods). At the global scale, this yields a total river network length surpassing 1.2 billion kilometres (excluding deserts and permanently glaciated regions, where channels are typically absent).

Given the ecological and biogeochemical value of non-perennial streams[20–25], it is crucial to identify, characterize and protect these segments of the global river network through targeted policy actions and tailored monitoring techniques[26–30]. This is especially urgent as climate change and river regulation are expected to increase the prevalence of such streams[31–35].

Currently, non-perennial reaches (that is, segments) are recognized as the most common type of rivers and streams worldwide[27–29,36,37]. The recent estimates by Messager et al.[38] serve as an important reference milestone in this area, suggesting that non-perennial streams

Department of Civil, Environmental and Architectural Engineering, University of Padova, Padova, Italy. ✉e-mail: gianluca.botter@dicea.unipd.it

https://doi.org/10.1038/s44221-025-00549-x

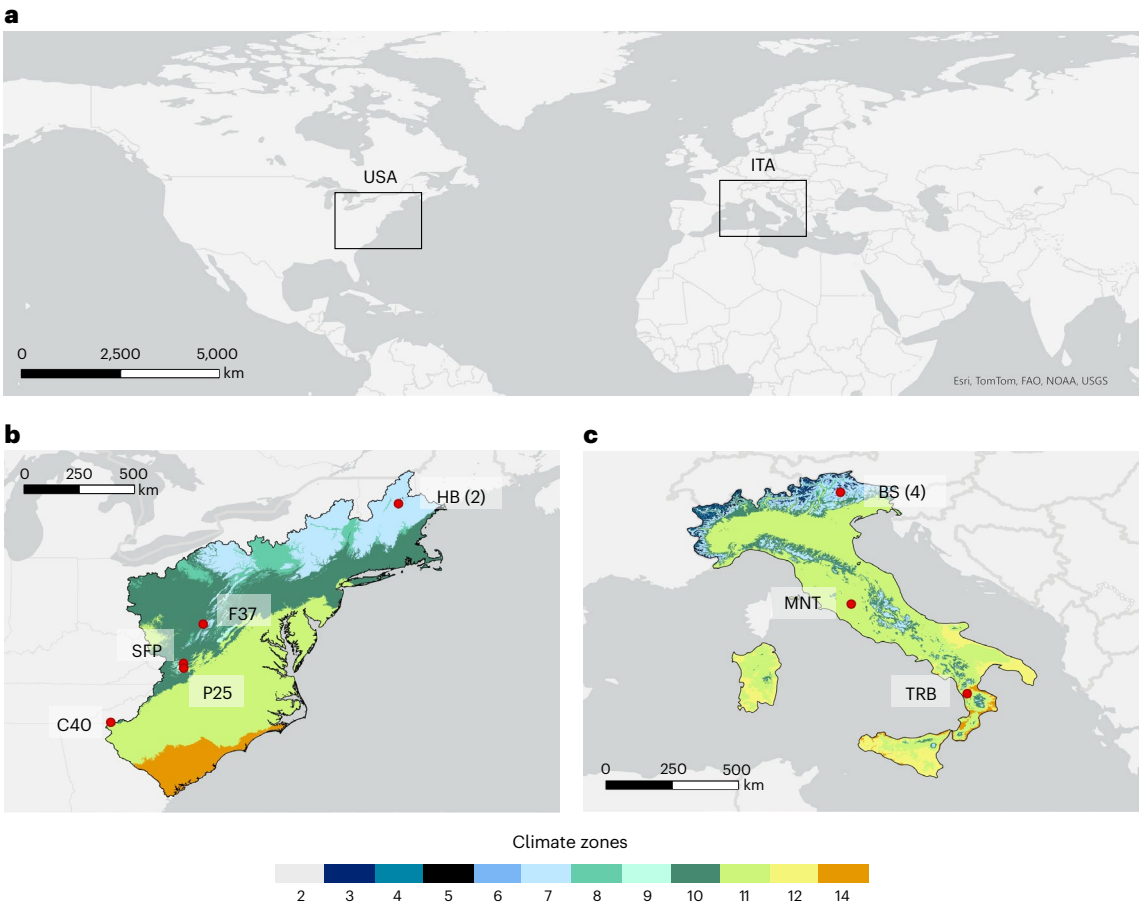

Fig. 1 | Study catchments and focus regions. a, The geographical position of the two macroregions considered in this study: Italy (ITA) and the eastern USA. **b**,**c**, Maps showing the geographical location of the study catchments within each macroregion. The numbers in parentheses indicate the number of catchments considered for each site. The colour codes represent different CZs, as follows: 2, Arctic (type II); 3, extremely cold and wet (type I); 4, extremely cold and wet (type II); 5, cold and wet; 6, extremely cold and mesic; 7, cold and mesic; 8, cool temperate and dry; 9, cool temperate and xeric; 10, cool temperate and moist; 11, warm temperate and mesic; 12, warm temperate and xeric; 14, hot and dry (Metzger et al.[58]). The study sites along with their acronyms and corresponding CZs are as follows: HB, Hubbard Brook 25 and 42 (CZ 7); F37, Fernow 37 (CZ 10); SFP, South Fork Potts (CZ 10); P25, Poverty 25 (CZ 10); C40, Coweeta 40 (CZs 8, 10 and 11); BS, Biois (CZs 3, 5, 6 and 7); MNT, Montecalvello (CZ 11); TRB, Turbolo (CZs 11 and 14). Maps created with ESRI ArcGIS Pro.

account for between 51% and 60% of the global river network by length. However, these estimates do not fully account for the role of headwater streams, which are typically more abundant and dynamic than higher-order streams. Specifically, the global estimate of Messager et al.[38] relies on streamflow data gathered in several near-natural gauging stations (Methods), which are used to extrapolate stream length and non-perennial flow fractions across 465 spatial subunits worldwide. However, the study refers to a global river network length that varies between 23 and 64 million kilometres, depending on the streamflow threshold used for identifying the channel network domain. This represents less than 6% of the global river network length, assuming a reference mean drainage density D_d of 10.48 km of channels per square kilometre (see Supplementary Table 3, where we also examine how sensitive this percentage is to the chosen drainage density).

The core idea of our work is that determining the fraction of non-perennial streams within a river network is a scale-dependent problem, as results are heavily influenced by the degree of detail used to define the channel network and the watershed size[39]. Yet, the dependence of the perennial fraction of river networks on the underlying channel initiation threshold remains underexplored, and the role of headwaters in shaping the fraction of non-perennial channels in large basins or regions is not fully understood, despite the growing availability of empirical datasets on stream expansion and retraction in small upland watersheds[3,40,41].

In this study, we combine theoretical analysis, model results and a dataset from 12 headwater catchments in Italy and the USA (Fig. 1) to address the following key questions: (1) To what extent is the fraction of non-perennial streams in large basins controlled by the headwaters? and (2) What changes can we expect in current estimates of the proportion of non-perennial streams across different basins and regions when the headwaters are comprehensively accounted for?

Scaling model for network- and catchment-scale temporariness

Regardless of the specific hydrological processes determining the underlying flow intermittency, a non-perennial (that is, temporary) channel is defined here as a stream that ceases to flow or dries out for at least one day per year on average[38]. The total temporary fraction (T_f) represents the proportion of non-perennial channels by length within a given area, considering all channels in that region. To better understand the fraction of non-perennial streams in a hydrological system, we focus on two different but related metrics: catchment-scale temporariness (ϕ_C) and network-scale temporariness (ϕ_N). Both metrics crucially depend on the contributing area, A—the upstream drainage area that contributes to the discharge of a stream (Fig. 2) and are described below:

- Network-scale temporariness, $\phi_N(A)$, represents the fraction of non-perennial streams in a river network, considering only reaches

https://doi.org/10.1038/s44221-025-00549-x

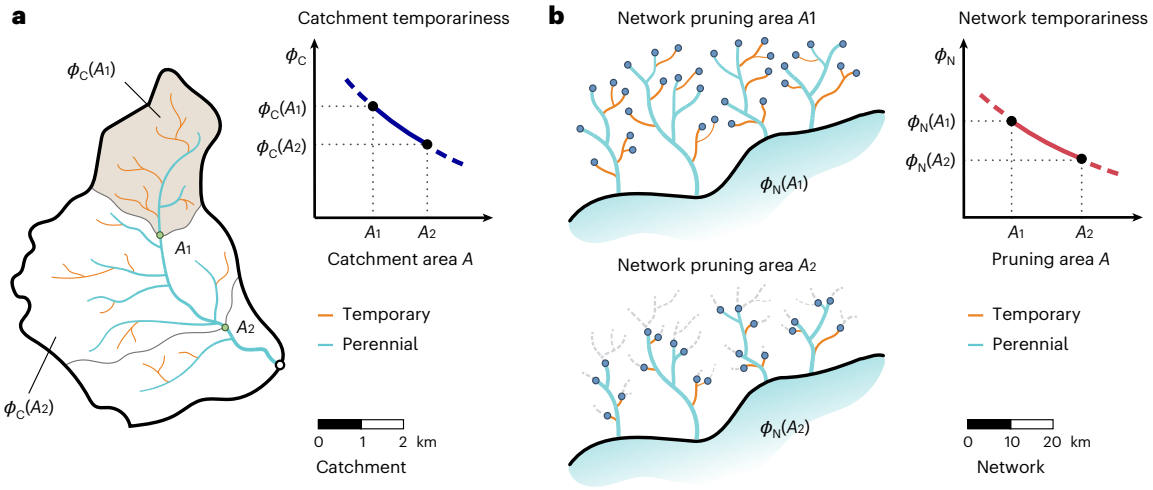

Fig. 2 | Conceptual representation of network and catchment temporariness, $\phi_N(A)$ and $\phi_C(A)$. a, Catchment-scale temporariness, $\phi_C(A)$: this represents the fraction of non-perennial streams among all river channels with a contributing area smaller than A. Crucially, as the reference catchment area A changes, the fraction of non-perennial streams also varies. In this example, a larger watershed encompasses a smaller proportion of non-perennial streams, and the catchment-scale temporariness ϕ_C decreases with A. **b**, Network-scale temporariness, $\phi_N(A)$. This represents the fraction of non-perennial streams among all channels with a contributing area greater than A. As the pruning area increases, the resolution of the network representation decreases. In this example, the network-scale temporariness $\phi_N(A)$ decreases with increasing pruning area, as larger channels tend to be more perennial.

with a contributing area larger than A. ϕ_N is commonly used in regional and global studies[38,42–46], which focus on vaster territories but sacrifice some spatial detail by using a larger threshold area A for the description of the network. This metric helps estimate how the temporary fraction within a river network changes with the underlying network drainage density;

- Catchment-scale temporariness, $\phi_C(A)$, looks at the fraction of non-perennial streams within a catchment or region, but only for reaches with a contributing area smaller than A. When viewed as a function of A, the catchment-scale temporariness shows how the proportion of non-perennial reaches changes with the watershed size. This metric is more suitable for detailed local studies, where stream dynamics can be observed with a higher level of detail (including all the headwaters).

In past studies, network-scale temporariness (ϕ_N) and catchment-scale temporariness (ϕ_C) have been evaluated only at specific points of their domain using preselected values of contributing area A. For example, Messager et al.[38] estimated ϕ_N for $A \approx 10$ km^2 (Supplementary Fig. 4) and used this value to extrapolate and infer the temporary fraction of the global river network, T_f. Similarly, ϕ_C has been calculated empirically only at the outlet of a few headwater catchments, where experimental data on stream network dynamics are available[3,47–50].

One important issue is that point-wise values of ϕ_N and ϕ_C should not be automatically assumed to be good proxies for T_f. Specifically, $\phi_N(A)$ approaches the total temporary fraction only when A is close to A_{min}, the actual contributing area of the channel heads, meaning even the smallest stream reaches are included. Likewise, $\phi_C(A)$ approaches the total temporary fraction only when the entire area of the focus catchment or region is considered (that is, for large values of A). Therefore, inferring T_f on the basis of available ϕ estimates is not straightforward and necessitates some extrapolation. This Article uses the concept of scaling to understand how the temporary fraction varies with catchment size and channel initiation threshold. Specifically, we analyse patterns of ϕ_N across large domains (including the world, Italy and the eastern USA) using existing model simulations[38], alongside empirical patterns of ϕ_C from our 12 study catchments (Methods). We then use a dual scaling model to extrapolate network (ϕ_N) and catchment (ϕ_C) temporariness beyond their respective observed domain (that is, for small pruning areas and large contributing areas) using a common set of parameters. These extrapolations, in turn, enable us to infer the total temporary fraction T_f for the selected study regions and the relevant river basins.

Furthermore, our analytical framework demonstrates that T_f can be represented as a weighted average of ϕ_N and ϕ_C evaluated at the same contributing area. This highlights the need to jointly model these two functions when inferring T_f, particularly when the pruning area is too coarse or the catchment area too small. From this perspective, our theoretical framework helps reconcile the scale mismatch between catchment and network temporariness (namely, the unavailability of ϕ_N at small values of A, and of ϕ_C at large values of A). Importantly, it also provides a robust and objective framework for quantifying the relative contributions of headwaters (ϕ_C) and larger streams (ϕ_N) to the overall temporary fraction of a river network.

Results

Scaling of the proportion of non-perennial streams

Analysing the patterns of network-scale temporariness across vast domains is challenging due to the limited availability of spatially distributed data on stream intermittency covering all the branches of large river networks. To address this, we leverage the output from the modelling study by Messager et al.[38]—referred to hereafter as the Global Intermittent Rivers and Ephemeral Streams (GIRES) dataset—to examine network temporariness across three study regions: the entire world, Italy and the northeastern USA (Fig. 3). The values of ϕ_N derived from the GIRES dataset exhibit a clear monotonic pattern in all cases: the smaller the network pruning area, the higher the fraction of non-perennial streams by length. The scaling pattern emerging in the GIRES dataset is disrupted only for contributing areas smaller than 10–20 km^2 (semi-transparent circles). Below this point, the value of ϕ_N derived from the GIRES dataset remains nearly constant due to the limited number of channels with $A < 10$ km^2 included in the network domain (representing only 6.7% of the total length considered).

Our analytical model (equation (1)) closely replicates the decreasing trend of $\phi_N(A)$ emerging from the GIRES dataset across the three focus regions (with R^2 approaching 1 in all cases). Extrapolating ϕ_N for contributing areas smaller than 10 km^2 using our scaling model shows that including small headwater channels in the calculation leads to a marked increase in the fraction of non-perennial streams. Although the x axis is logarithmic, with intervals on the left representing

https://doi.org/10.1038/s44221-025-00549-x

progressively smaller changes in A, the variations in ϕ_N remain consistent across all contributing areas explored, indicating a markedly convex decay of network temporariness with the pruning area[51]. This is because low-order streams are consistently more dynamic and abundant than higher-order channels[8,52], notably influencing the overall temporary fraction of larger basins across a wide range of channel initiation thresholds.

Unlike network-scale temporariness, catchment-scale temporariness can be analysed empirically in sites where observations on network expansion and contraction are available. To this aim, here we leverage empirical data from 12 catchments in Italy and the USA encompassing diverse climatic and hydrologic conditions. The selection includes sites where stream intermittency has been measured with sufficient spatial and temporal resolution, although hot and dry climates are not represented. The empirical patterns of catchment-scale temporariness, ϕ_C, across our study sites reveal a generally monotonically decreasing trend (Fig. 4). Our analytical model reasonably captures the observed patterns of $\phi_C(A)$ (with a mean R^2 exceeding 0.80). While some scatter in the experimental data suggests the potential presence of non-monotonic patterns in catchment temporariness, the overall trend indicates that larger basins have a higher proportion of perennial streams compared with their smaller subcatchments, in line with what is predicted by the analytical model. Although the notion that smaller streams are more dynamic and less perennial than larger rivers is certainly intuitive, this study provides rigorous empirical and theoretical support for it.

The modelled catchment-scale temporariness, ϕ_C, has been also extrapolated for contributing areas larger than those where empirical data have been collected (Fig. 4). In the extrapolation, it is assumed that the scaling patterns observed in the headwaters also hold for larger channels and for the new headwaters draining into them. In all cases, the rate of decrease of the catchment-scale temporariness diminishes as the contributing area increases. Consequently, the relative changes in $\phi_C(A)$ become smaller for larger contributing areas, with $\phi_C(A)$ approaching a nearly flat behaviour as A reaches 10 km^2. This behaviour stems from the disproportionate length of small streams compared with large channels and tends to emerge from both the empirical observations and the scaling model in most of the circumstances examined in this study.

Temporary fractions estimates

The ability of the model to accurately reproduce the patterns of $\phi_N(A)$ and $\phi_C(A)$ from both experimental data and the the GIRES dataset indicates it can offer reasonable predictions of the total temporary fraction T_f in different basins or regions by extrapolating the trends exhibited by the network and catchment temporariness.

Inferring T_f by extrapolating the network temporariness $\phi_N(A)$ requires caution, as the result is potentially sensitive to the chosen value of the channel initiation threshold, A_{min} (Fig. 3). This threshold controls the extent of the modelled channel network and is typically calibrated to match observed drainage density in a given region. Although the exact length of the world's river network cannot be determined, we adopt a representative range for the global mean drainage density of 10.48 ± 1.13 km km^{-2}, derived from a statistical analysis of previously published data (Methods). Under this assumption, extrapolating the GIRES dataset yields a global temporary fraction of 0.767 ± 0.021 to 0.784 ± 0.020 (Table 1). These values reflect uncertainty in the model parameters and the value of global network length. Interestingly, the sensitivity of T_f to drainage density is relatively limited within the range of D_d values in line with empirical observations (Supplementary Information Section 5.5). This aggregated estimate was complemented by a disaggregated analysis that subdivided the world into 60 river basins, to account for spatial variability in both the shape of $\phi_N(A)$ and D_d (that is, A_{min}). The disaggregated estimate yields a range of T_f from 0.728 ± 0.011 to 0.736 ± 0.010 depending on the reference mean global drainage density, slightly lower than the corresponding

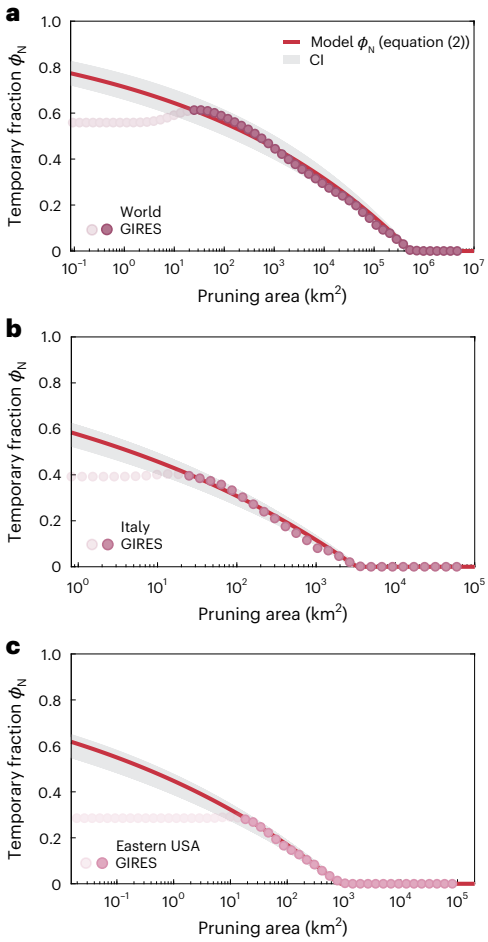

Fig. 3 | Scaling of the network-scale temporariness. a–c, The GIRES dataset was analysed to estimate the fraction of non-perennial streams in river networks characterized by different pruning areas, $\phi_N(A)$. The three plots represent different regions: the entire world (**a**), Italy (**b**) and the eastern USA (**c**). Circles represent the results of calculations based on the GIRES dataset, with transparent ones indicating pruning areas below 20 km^2, where the the GIRES dataset does not include the expected number of reaches owing to the limited resolution of the network domain. These points are fitted with the modelled ϕ_N (red line, equation (2), R^2 = 0.99 in all cases) and extrapolated to lower pruning areas, down to the point where the drainage density equals 10.48 km km^{-2}. The confidence interval (CI) for the fitting is also shown. This CI refers to the ensemble of all the model predictions fulfilling the minimum performance criteria defined in Supplementary Information Section 4.2. This approach enables the calculation of the total temporary fraction, T_f, as the intercept of the red line with the vertical line $A = A_{min}$: $T_f \approx 0.78$ globally (**a**), $T_f \approx 0.59$ in Italy and $T_f \approx 0.62$ in the eastern USA.

aggregated estimate. The spatial patterns of the temporary fraction derived from the disaggregated estimate are shown in Fig. 5 and reveal a clear climatic signature. The highest T_f values are concentrated in Africa and Australia. By contrast, the lowest values of temporary fraction occur in Northern Europe, some major Asian-Pacific islands (including New Zealand and the Philippines) and the Amazon basin. Both Asia and the Americas display pronounced internal heterogeneity of temporary fraction, with a wide range of T_f across different basins. Although the geographic distribution of T_f might be impacted by the spatial patterns of D_d, the global T_f value shows a limited sensitivity to the observed D_d heterogeneity. Indeed, assuming a spatially uniform drainage density all over the world, yields analogous results for the global T_f (Supplementary Table 6). The disaggregated approach effectively captures existing heterogeneity in climate and geomorphological features, which are reflected in a multimodal frequency distribution of T_f (Fig. 5, inset); however, model performance is poorer as compared

https://doi.org/10.1038/s44221-025-00549-x

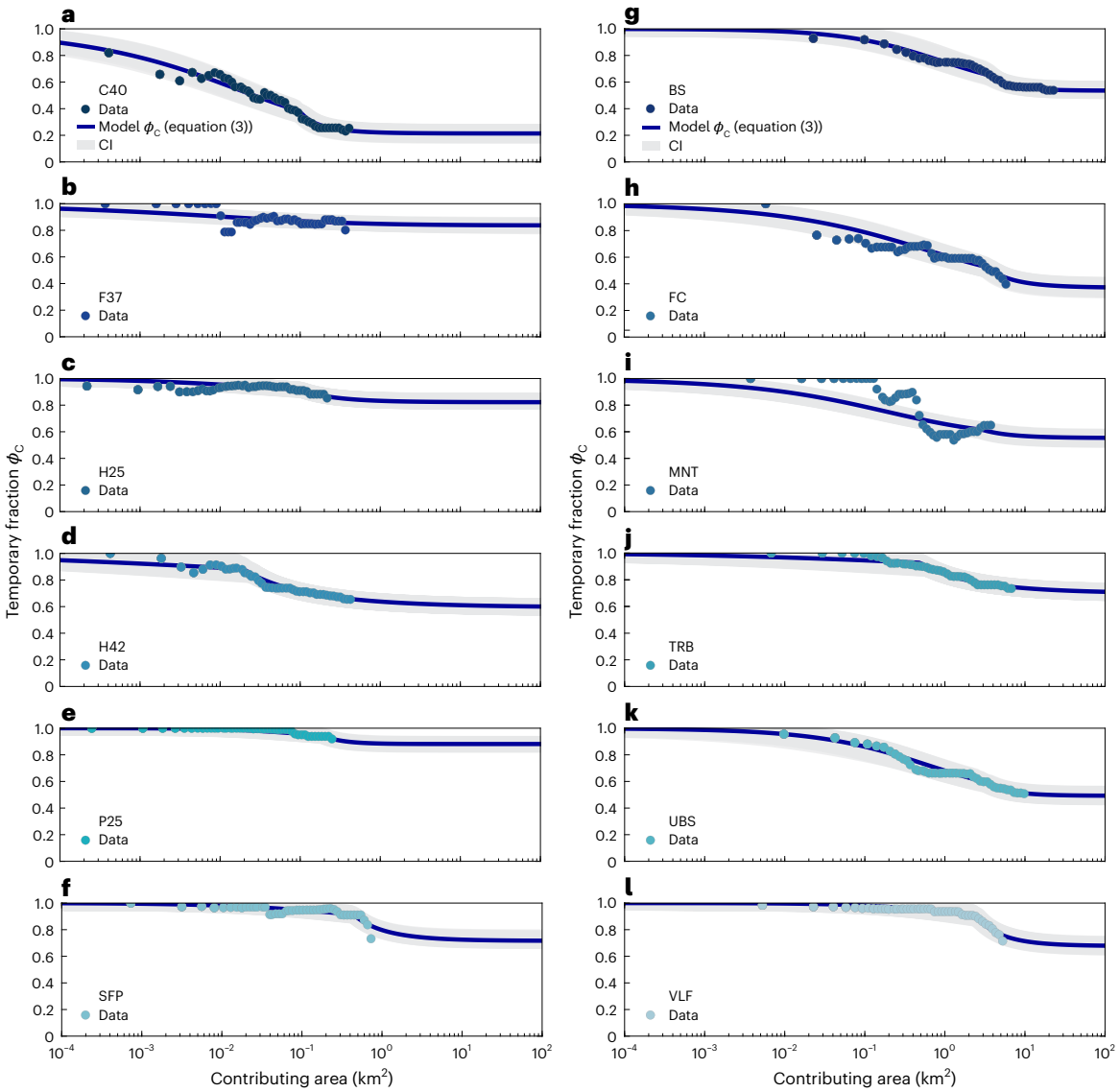

Fig. 4 | Scaling of the catchment-scale temporariness. a–l, The values of ϕ_C, obtained from empirical data for each study catchment, are plotted against the contributing area A (circles). The x position of the leftmost dot within each panel indicates the contributing area of the smallest channel heads observed in that catchment. Although A_{min} varies across catchments, the same x-axis range is used for all panels for comparability. The experimental data are interpolated with the modelled catchment temporariness $\phi_C(A)$, as given by equation (3), over a range of contributing areas from 10^{-4} to 10^2 km^2. Each modelled curve (continuous lines) is accompanied by a confidence interval (CI), shown as a grey-shaded area. This CI refers to the ensemble of all the model predictions fulfilling the minimum performance criteria defined in Supplementary Information Section 4.2. The model effectively captures the decreasing trend of the temporary fraction with increasing A. **a–l** correspond to the 12 study catchments, identified by their acronyms, as labelled in the figure. The coefficient of determination (R^2) for each study catchment is as follows: R^2(C40) = 0.96 (**a**), R^2(F37) = 0.26 (**b**), R^2(H25) = 0.70 (**c**), R^2(H42) = 0.96 (**d**), R^2(P25) = 0.78 (**e**), R^2(SFP) = 0.71 (**f**), R^2(BS) = 0.98 (**g**), R^2(FC) = 0.88 (**h**), R^2(MNT) = 0.49 (**i**), R^2(TRB) = 0.96 (**j**), R^2(UBS) = 0.96 (**k**) and R^2(VLF) = 0.97 (**l**) (Supplementary Table 4).

with the aggregated estimate, especially in regions with limited data and scattered network temporariness (Supplementary Fig. 11). This circumstance may limit the robustness of the extrapolation procedure in the disaggregated scenario.

In all the scenarios explored, the resulting value of temporary fraction is notably higher than the range of 0.51–0.60 suggested by Messager et al.[38]. Although based solely on the GIRES dataset, our extrapolation probably improves upon previous assessments as they are grounded on a more consistent and realistic representation of the global river network length.

When calculating T_f from the extrapolation of $\phi_N(A)$ at the regional scale, uncertainty in the representative channel initiation threshold increases further. Drainage density can vary substantially with climate and geological characteristics and regional values should be calibrated to local landscape properties. To overcome this challenge, for Italy and the eastern USA, we adopted a conservative approach by using the average drainage density observed within the study catchments of each region, as these values are lower than the corresponding global mean. Even in this conservative scenario, the T_f estimates for the eastern USA (0.62 ± 0.02) and Italy (0.59 ± 0.01) are significantly higher than those reported by Schneider et al.[43] (0–0.25 for both regions) and those inferred from the the GIRES dataset in the case of 32 million kilometres of channel (T_f = 0.29 for the USA, T_f = 0.36 for Italy)[38]. In all three macroregions, the relative contribution of $\phi_N(A \approx 10$ km$^2)$ to T_f is on average 5%, suggesting that unaccounted headwaters mainly determine the actual value of temporary fraction due to the dominance of low-order streams in the regional or global channel network.

https://doi.org/10.1038/s44221-025-00549-x

Table 1 | Study catchments and regions along with their key hydromorphological attributes

Catchment	A_{max} (km^2)	A_{min} (km^2)	L_{net} (km)	D_d (km^{-1})	$T_f \pm \sigma$
Coweeta 40 (C40)	0.41	0.044	2.55	6.26	0.218±0.009
Fernow 37 (F37)	0.37	0.049	1.73	4.72	0.839±0.006
Hubbard Brook 25 (H25)	0.22	0.008	3.08	14.20	0.824±0.005
Hubbard Brook 42 (H42)	0.42	0.001	4.27	10.06	0.590±0.004
Poverty 25 (P25)	0.25	0.040	1.91	7.68	0.893±0.008
South Fork Potts (SFP)	0.73	0.077	2.09	2.87	0.711±0.010
Biois (BS)	22.75	0.908	46.73	2.05	0.538±0.007
Fuciade (FC)	5.85	0.928	8.04	1.37	0.370±0.011
Montecalvello (MNT)	3.75	0.385	6.09	1.62	0.549±0.007
Turbolo (TRB)	6.78	0.032	39.97	5.90	0.697±0.006
Upper Biois (UBS)	9.78	0.816	18.98	1.94	0.492±0.009
Valfredda (VLF)	5.27	0.737	16.97	3.22	0.674±0.007
Region					
World aggregated	1.32×10^8	0.216	1.231×10^9	9.35	0.767±0.021
		0.111	1.380×10^9	10.48	0.775±0.023
		0.025	1.529×10^9	11.61	0.784±0.020
World disaggregated	1.32×10^8	0.154*	1.231×10^9	9.35	0.728±0.011
		0.142*	1.380×10^9	10.48	0.731±0.011
		0.131*	1.529×10^9	11.61	0.736±0.010
Italy	3.01×10^5	0.818	8.10×10^5	2.69	0.585±0.014
Eastern USA	6.98×10^5	0.016	5.33×10^6	7.63	0.617±0.020

The first column provides the name and acronym of each catchment or region. Columns 2 and 3 contain information on the maximum catchment size for which observations are available or the region size (A_{max}) and the representative value of the channel initiation threshold in the focus catchment or region (A_{min}), derived on the basis of the scaling of the channel length with pruning area by imposing the total network length in the target domain (column 3). Therefore, A_{min} changes across different regions, and is anticorrelated with the scaling exponent b. This explains the variability of the parameter across catchments, with the lowest A_{min} corresponding to the highest b. The values with the asterisks correspond to cases in which D_d is heterogeneous, for which the spatial average of the pruning areas across all basins is reported. Columns 4 and 5 contain information on the maximum flowing network length (L_{net}) and the associated geomorphic drainage density (D_d) based on the maximum network length. In the world, D_d is estimated on the basis of a sample built using literature data[3,12–19] and L_{net} is calculated accordingly (Methods). In Italy and the eastern USA, instead, we adopted a conservative approach where D_d is calculated as the average drainage density observed across all the study catchments belonging to the considered region. The final column presents the estimated temporary fractions, derived by extrapolating the modelled ϕ_C (for catchments) and ϕ_N (for regions).

An alternative method for estimating T_f involves extrapolating the observed catchment-scale temporariness, ϕ_C, for larger contributing areas (Fig. 4). The extrapolation results are presented in Fig. 6 and Table 1. For catchments in the USA, the estimated T_f values predominantly range from 0.59 to 0.89, with a mean of 0.68 and a single outlier (T_f = 0.22 for Coweeta 40). In the Italian peninsula, T_f spans from 0.37 to 0.70, with a mean of 0.55.

The T_f values derived from extrapolating ϕ_C should be interpreted with caution, as they do not represent the temporary fraction observed within each study catchment (ϕ_C evaluated for $A = A_{max}$), but the predicted temporary fraction for a larger watershed that includes one of our experimental sites in its headwaters. This prediction relies on the observed scaling of perennial and non-perennial lengths within the study catchments. However, our estimates assume the temporariness of headwaters across the entire basin or region reflects the network dynamics observed within our experimental sites, which may not hold due to spatial heterogeneity in geological, morphological and vegetation characteristics. For instance, extrapolating T_f in the Piave River basin (northeastern Italy), which encompasses four partially nested monitoring catchments with varying sizes, elevations and groundwater spring distributions, results in T_f values ranging from 0.37 (FC) to 0.67 (VLF), depending on the headwater site used for prediction (Table 1). From this perspective—although geology, climate and landscape characteristics may vary both locally and regionally—collecting empirical data on network dynamics in large watersheds (for example, A_{max} > 10–100 km^2) could increase the representativeness of headwater observations, thereby improving the reliability of T_f estimates based on ϕ_C extrapolations. Regardless of the specific values of T_f inferred from the catchment-scale temporariness, the scaling of network length with pruning area shows that headwaters (channels with a contributing area smaller than A_{max}) account for at least 84.4% of T_f in the US basins and 83.5% in the Italian basins (Supplementary Information Section 5.4). This highlights that headwaters are far more abundant than higher-order channels and strongly influence the total fraction of non-perennial streams across a wide range of catchment areas.

Although acknowledging the uncertainty regarding the representativeness of our experimental sites for larger-scale assessments, and aware that global analyses are not designed to capture subregional patterns, we believe comparing our basin-scale estimates of T_f with those of Messager et al.[38] is instructive. The extrapolated T_f values from the empirical $\phi_C(A)$ curves are consistently higher than the temporary fractions derived from the GIRES dataset for the river basins containing the study catchments (on average +0.29), in the scenario where the global river network spans 32 million kilometres. This discrepancy is particularly pronounced in the humid, cooler regions of Italy and the USA (BS, H25 and H42), where the the GIRES dataset suggests that almost all reaches of the network should be perennial.

Extrapolating catchment-scale T_f estimates to the regional level introduces additional uncertainty, due to the broader extent of the area under investigation. However, given the even geographical distribution of study sites across the focal regions, and their ability to capture the relevant climatic regimes within each region, we argue that these extrapolations provide a meaningful first-order approximation of the actual temporary fraction in Italy and the eastern USA. In fact, the

https://doi.org/10.1038/s44221-025-00549-x

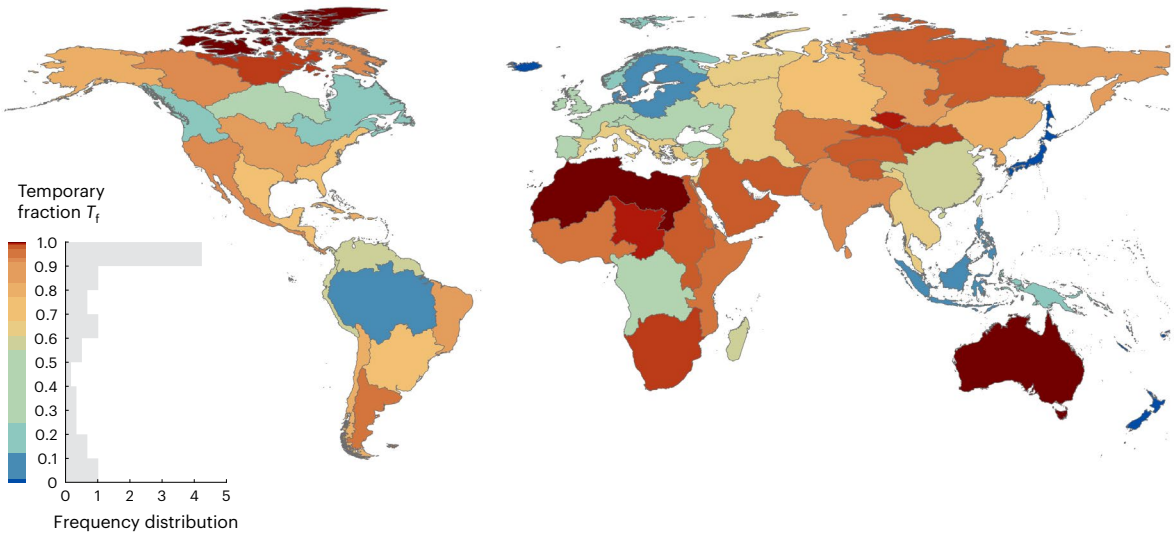

Fig. 5 | Global spatial patterns of temporary fraction T_f. The map reports the disaggregated T_f estimates for the 60 river basins delineated according to HydroBASINS (level 2)[59]. For each basin, ϕ_N was fitted independently and extrapolated to the corresponding A_{min}, yielding a basin-specific value of T_f. The inset shows the global frequency distribution of T_f, which is clearly multimodal, with the dominant mode at $T_f = 1$. Map created with ESRI ArcGIS Pro.

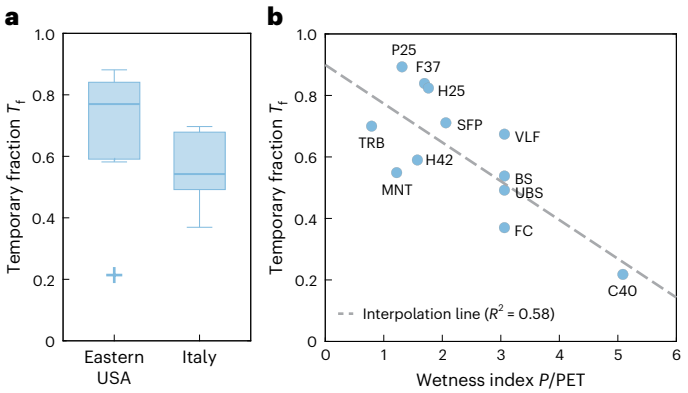

Fig. 6 | Estimate of the total temporary fraction T_f derived by extrapolating $\phi_C(A)$ in our 12 study catchments and relationship with climate. a, A box plot showing the distribution of temporary fractions (T_f) in the study catchments, separated by macroregion: the eastern USA (left) and Italy (right). The box plot for the eastern USA is based on six catchments, with a minimum outlier (cross symbol) of 0.21 and a maximum value of 0.88. The median is 0.77, while the 25th and 75th percentiles are 0.59 and 0.84, respectively. The box plot for Italy is based on six catchments, with a minimum value of 0.37 and a maximum of 0.70. The median is 0.54, while the 25th and 75th percentiles are 0.49 and 0.68, respectively. **b**, The relationship between the total temporary fraction and the wetness index, calculated as the ratio of mean annual precipitation (P) to mean annual potential evapotranspiration (PET). These P and PET values refer to the time periods where the surveys were conducted (Supplementary Information Section 1). Arid catchments tend to exhibit higher average T_f values. The linear regression is represented by the dashed line, with a coefficient of determination of $R^2 = 0.58$.

mean T_f values inferred from empirical data in our study catchments reasonably align with the corresponding regional estimates derived by extrapolating the $\phi_N(A)$ fitted on the the GIRES dataset to smaller streams (Fig. 3b,c and Table 1).

Interestingly, the T_f estimates based on ϕ_C show a clear dependence on the underlying hydroclimatic conditions, with higher values of T_f associated with more arid regions (lower catchment wetness index, calculated as the ratio between mean precipitation P and mean potential evapotranspiration PET). Our analysis confirms that sites with a greater abundance of excess water tend to have a higher proportion of perennial streams, in line with previous studies[2,50,51]. The scatter of experimental points in the T_f versus P/PET plot is moderate, suggesting that our basin-scale temporary fraction estimates primarily reflect the hydroclimatic regime of the area, with lower influence from site-specific factors (catchment size, drainage density and geological substrate). Notably, all sites with P/PET < 2.5 have an estimated total temporary fraction higher than 0.55. Given the widespread extent of water-limited and mid-humid areas globally (with approximately 90% of the land surface having P/PET < 2.5; Supplementary Fig. 14), our ϕ_C-based T_f estimates, grounded on local observations of network dynamics, confirms that non-perennial channels certainly represent the most common type of rivers globally.

Conclusions

Non-perennial rivers are not special types of rivers; rather, they reflect the widespread and natural occurrence of streamflow intermittency driven by hydroclimatic variability. Estimating the temporary fraction of a river network at large scales presents considerable challenges. Empirical data are scarce and mainly confined to headwaters, while global datasets that rely on discharge data from distributed monitoring networks fail to capture network dynamics in low-order streams. In this Article, we advance current large-scale estimates of the proportion of non-perennial streams in a river network by focusing on the pivotal role of headwaters. To achieve this, we leverage on a dual scaling model that enables extrapolation from upstream reaches to larger watersheds, as well as from high-order channels back to the headwaters, using the same set of parameters. The approach has been successfully applied to an existing global dataset (GIRES) and empirical observations gathered in 12 study sites. Our results indicate that headwaters consistently control the value of the temporary fraction across catchments of any size. This means that flow intermittency is not limited to upland, low-order streams; rather, the signature of channel wetting and drying in the headwaters persists even in bigger watersheds, owing to the abundance of such streams in large river networks. The present analysis also suggests that the global temporary fraction can be significantly higher than expected, reaching values in the range of 0.7–0.8 when low-order streams are adequately considered. Similarly, regional estimates of T_f in Italy and the eastern USA approach or surpass 0.6, consistent with extrapolations from the experimental sites considered in this study. The fraction of non-perennial streams in a river network displays a

strong climatic signature, with a dominant proportion of intermittent reaches in areas where P/PET < 2.5 (which accounts for roughly 90% of the global land surface). Overall, our work reveals that, when headwaters are comprehensively accounted for, non-perennial streams largely dominate the river network length, regionally and globally.

Methods

Estimation of global drainage density and characterization of the regional patterns of D_d

Because the exact value of drainage density (D_d) at the global scale cannot be directly determined, we compiled data from nine published experimental studies reporting empirical measurements of D_d across diverse climatic and geographic settings[3,12–19]. This produced a dataset of $N = 344$ individual observations of D_d. We analysed this sample using the maximum likelihood method to estimate the sample mean and its associated uncertainty, obtaining a mean D_d of 10.48 ± 1.13 km km^{-2}, where the uncertainty corresponds to $1.96\,\sigma/\sqrt{N}$, with σ being the sample standard deviation. This value should be regarded as an estimate of the global value of D_d rather than an exact figure. Nevertheless, it represents the most objective approach available to approximate a global average drainage density from existing empirical evidence. The full frequency distribution of D_d is shown and discussed in Supplementary Information Section 5.1. In the disaggregated scenario, where D_d varies spatially across different basins, catchment-specific drainage density values were obtained from the global map delivered by Lin et al.[53], rescaled by a multiplicative factor to match the selected global average of D_d.

General relationship among network temporariness, catchment temporariness and total temporary fraction

In this study, we assume that the overall river network domain is fixed and known (the so-called geomorphic river network). Moreover, we postulate that each network segment can be classified as either non-perennial (if the stretch dries out for at least one day per year on average) or perennial (if it dries out for less than one day per year on average). Consequently, the total length of the river network, L, consists of two additive and complementary components: the non-perennial, temporary length, L_t, and the perennial length, L_p, such that $L = L_t + L_p$. In this vein, the total temporary fraction of a channel network, T_f, is defined as the ratio of the temporary to the total length, that is, $T_f = \frac{L_t}{L} = 1 - \frac{L_p}{L}$.

In a similar vein, the total river network length, L, can be decomposed into the length of streams with a contributing area smaller than A (that is, those within subcatchments with area smaller than A), denoted as $L_C(A)$, and the length of channels with a contributing area larger than A (that is, those in a network extracted using the pruning area A), denoted as $L_N(A)$. This decomposition is expressed as: $L = L_C(A) + L_N(A) = \text{const}$. By combining the decomposition with the definition of T_f, we obtain the following equation, which is valid for any arbitrary contributing area A above the contributing area of the channel heads A_{min} (Supplementary Information Section 3.3):

$$L\ T_f = L_C(A)\,\phi_C(A) + L_N(A)\,\phi_N(A), \quad (1)$$

where $\phi_C(A)$ and $\phi_N(A)$ represent the catchment and network temporariness, respectively. This equation shows that the total temporary fraction can be expressed as a weighted average of the catchment and network temporariness, evaluated at the same contributing area A. The weights are represented by the fractions of network length with contributing areas smaller and larger than A, respectively. For instance, if, for $A = 10$ km^2, the ratio $L_N(A)/L \approx 0.15$, it could be concluded that the relative contribution of ϕ_N to T_f at 10 km^2 is only 15%, because the value of ϕ_N incorporates only 15% of the total network length. The weight functions $L_N(A)$ and $L_C(A) = L - L_N(A)$ on the right-hand side of equation (1) are determined by fitting a power-law scaling to the modelled and observed relationships between channel network length and pruning area, while accounting for finite size and coarse-graining effects where applicable (Supplementary Fig. 8).

Study catchments

To better understand the role of headwaters in shaping the temporariness of large-scale river networks, we use experimental data gathered in 12 headwater catchments in Italy and the eastern USA. These sites encompass the majority of existing experimental catchments where data on stream network dynamics have been collected with sufficient spatial resolution and full spatial coverage, and are openly available. Although we recognize that extremely dry and arid sites are not included in the selection, the catchments span a range of latitudes (approximately 35° to 46° N) and altitudes (from 89 to 3,000 m a.s.l.), and are distributed across seven diverse climatic zones (CZs 3, 5, 6, 7, 10, 11 and 14; see the caption of Fig. 1). Their contributing areas vary from 22 ha to 23 km^2, and their maximum drainage density (calculated when the network is fully expanded) falls in the range of 1.37–14.20 km km^{-2} (mean 5.1 km km^{-2}). At these experimental sites, the active portion of the river network has been mapped multiple times (at least seven times) under highly variable hydrological conditions (for example, wet versus dry), enabling the estimation of the spatial distribution of local persistency, namely the percentage of time during which each branch of the river network is actively flowing.

GIRES dataset

The dependence of the network's temporary fraction on the pruning area is assessed across different large-scale domains (Italy, the eastern USA and the entire globe) using the GIRES dataset developed by Messager et al.[38]. This model offers the most up-to-date and widely recognized estimates of the temporary fraction at both global and regional scales. It is based on a global digital river network constructed from geospatial information in the RiverATLAS and HydroATLAS datasets, using a digital terrain model with a grid size of 15 arc-seconds (approximately 500 m at the Equator). The channel network domain is defined by pixels that meet one of the following criteria: (1) the pixel has an upstream watershed area greater than 10 km^2 or (2) the pixel has a long-term average natural discharge (mean annual flow) exceeding 0.1 m^3 s^{-1}. The above criteria were applied globally to define the river network across all continents, except Antarctica (Supplementary Information Section 2), resulting in a total network length of 23 million kilometres. A random forest model was then applied to calculate the probability of flow intermittence for each reach of the network, which was eventually used for classifying these reaches as either 'perennial' or 'non-perennial'. The model predictors include variables describing climate, physiography, land cover, soil, geology and hydrology. The training and cross-validation use spatially distributed discharge data on mean annual flow derived from 5,615 streamflow gauging stations worldwide. Although this sample may not fully represent natural hydrological conditions, the work by Messager et al.[38] offers a reliable estimate of temporary river fractions, based on gauging stations selected to reflect near-natural conditions. The analysis of the distribution of the network length L_N with A (Supplementary Information Section 2) indicates that headwaters are underrepresented in the the GIRES dataset, with channels having contributing areas lower than 10 km^2 accounting for only 6.7% of the total network length. This underrepresentation also persists in the extrapolation scenario where the total network length is increased to 64 million kilometres. In this case, in fact, the drainage density of the the GIRES dataset (0.48 km km^{-2}) remains one order of magnitude lower than the actual drainage density observed in the field (Table 1).

Reconstructing the patterns of network and catchment temporariness from empirical data and model simulations

Catchment-scale temporariness, $\phi_C(A)$, is derived for each study catchment using empirically based maps of local persistency (representing

the percentage of time a reach remains flowing). To estimate $\phi_C(A)$, we first analyse the empirical estimates of the persistencies of each reach within the study catchments and classify each reach as either perennial or non-perennial. Following Messager et al.[38], we define a reach as non-perennial if it dries out on average at least one day per year, and as perennial otherwise. Accordingly, reaches with a persistency equal to or greater than 0.99 are classified as perennial, while all others are considered non-perennial. The contributing area for each reach of the network is then calculated on the basis of a digital terrain model of the area (resolutions ranging from 1 to 5 m), which has been made consistent with the network itself (Supplementary Information Section 1). Finally, the function $\phi_C(A)$ is calculated as the ratio of the length of non-perennial channels with a contributing area smaller than A to the total length of the network having a contributing area smaller than A (Supplementary Information Section 3.1). This computation is repeated by varying A from the minimum area of the channel heads, A_{min}, up to the catchment area at the outlet, A_{max}.

Similarly, the network-scale temporariness, $\phi_N(A)$, is derived by analysing the reach-scale classification in the GIRES output as either non-perennial or perennial, along with the corresponding cumulative area associated to each river segment within our focus regions. The network temporariness, $\phi_N(A)$, is then computed as the ratio of the length of non-perennial channels with contributing area greater than A to the total length of channels with contributing area greater than A (Supplementary Information Section 3.2). This calculation is repeated by varying A from the minimum contributing area of the network to the total catchment or region area. In the analysis, only reaches with a contributing area greater than 20 km^2 were considered for identifying the scaling of $\phi_N(A)$, to account for the limited number of reaches with smaller values of contributing area included in the GIRES domain.

Scaling model for $\phi_N(A)$ and $\phi_C(A)$

To reproduce and extrapolate observed patterns of network and catchment temporariness, we assume that the network domain can be defined using an appropriate threshold for the contributing area and introduce a scaling model that relates network length to the pruning area, A. This model is inspired by geomorphological studies, which suggest the existence of a power-law relationship between the channel network length, L_N, and the corresponding head pruning area A, of the form $L_N(A) = a\,A^{-b}$, where a and b are constants[17,52,54]. In this study, the model is extended to the perennial length of the river network, $L_{p,N}(A)$, which is assumed to follow the same type of power-law scaling exhibited by the network length L_N: $L_{p,N}(A) = cA^{-d}$. Both these relationships are assumed to be valid in a given catchment or region for A ranging from the minimum pruning area A_{min} to the total area of the catchment or region, A_{max}. Under the above assumptions, the catchment and network temporariness can be analytically expressed as follows:

$$\phi_N(A) = 1 - k\,(A)^{b-d}, \tag{2}$$

$$\phi_C(A) = 1 - k\,(A_{min})^{b-d}\left[\frac{1-(A/A_{min})^{-d}}{1-(A/A_{min})^{-b}}\right], \tag{3}$$

where $b, d, k = c/a$ and A_{min} are the catchment- or region-specific model parameters. The above analytical expressions need to be corrected as detailed in Supplementary Information (Supplementary Equations (8) and (12)) in cases where $L_{p,N}(A) = L_N(A)$ for $A < A_{max}$ (that is, if the network is completely perennial above a threshold contributing area). Of the five model parameters, a and b are fitted to the reconstructed functions $L_N(A)$ (either derived from empirical data or from the GIRES dataset). In addition, for our study, catchments c and d are fitted to the functions $\phi_C(A)$ derived from empirical data. Instead, for the macroregions, c and d are fitted to the function $\phi_N(A)$ obtained from the GIRES dataset analysis. Finally, A_{min}, which represents the typical channel initiation area in the focus region, is determined on the basis of the observed (or estimated) drainage density D_d from the equation $L_N(A_{min}) = a\,A_{min}^{-b} = D_d\,A_{max}$. Accordingly, A_{min} depends on D_d, b and A_{max}/a and may vary considerably across different catchments or regions, even when they are nested. In the calibration process, we use an informal Informal Generalized Likelihood Uncertainty Estimation[55] approach to identify the optimal set of model parameters and their corresponding confidence intervals.

Extrapolating network and catchment temporariness to estimate T_f

The equations derived for catchment-scale and network-scale temporariness enable the estimation of the total temporary fraction of a given catchment or region using a straightforward analytical approach, as detailed below. Specifically, the temporary fraction T_f, by definition, can be interpreted as the limit of $\phi_C(A)$ as the contributing area A approaches the size of the focus region, ensuring that all channels in the region are accounted for. Similarly, T_f can be viewed as the limit of $\phi_N(A)$ as A tends to the minimum support area of the network, A_{min}, ensuring that all headwaters are comprehensively accounted for. Thus, provided that $A_{max} \gg A_{min}$, the total temporary fraction of a river network can be expressed as

$$T_f = \lim_{A\to A_{max}} \phi_C(A) = \lim_{A\to A_{min}} \phi_N(A) = 1 - k\,[A_{min}]^{b-d}, \tag{4}$$

which is amenable to analytical evaluation. When T_f is inferred from the extrapolation of $\phi_N(A)$, the estimation procedure depends on the nature of the estimate (aggregated versus disaggregated) and the underlying spatial patterns of drainage density. In the aggregated case, where D_d is uniform across the target domain, the aggregated $\phi_N(A)$ function is extrapolated to A_{min}. In heterogeneous scenarios, by contrast, each basin-specific ϕ_N is extrapolated individually, using spatially variable A_{min} values that reflect the imposed distribution of D_d (see 'Estimation of global drainage density and characterization of the regional patterns of D_d' section). The procedure of extrapolating $\phi_N(A)$ to infer T_f is similar to that devised by Messager et al.[38], with two key differences: (1) it uses scaling laws based on contributing area instead of mean annual flow (which is harder to assess), and (2) the extrapolation incorporates a larger number of small channels, better aligning with the actual drainage densities of rivers and fully capturing the influence of the headwaters. Interestingly, in all cases, $\phi_N(A)$ remains considerably different from T_f unless A is very close to A_{min}, while $\phi_C(A)$ converges to T_f at relatively low values of the contributing area (approximately $A \approx 10$–100 km^2). This suggests that using $\phi_C(A)$ to approximate T_f may be a more robust approach than truncating $\phi_N(A)$ at relatively large pruning areas.

Reporting summary

Further information on research design is available in the Nature Portfolio Reporting Summary linked to this article.

Data availability

The river network used to derive the Italian, American and global datasets is available via figshare at https://doi.org/10.6084/m9.figshare.14633022 (ref. 56). Data used to carry out these analyses are available at https://researchdata.cab.unipd.it/id/eprint/1539 (ref. 57). This repository contains both the data collected for the study catchments and the shapefiles used to extract the river networks of Italy and the eastern USA.

Code availability

Geospatial analyses were performed using ESRI ArcGIS Pro (version 3.3.0) and the MATLAB programming language (version R2024a), while figures were prepared using Adobe Illustrator CC 2015. The MATLAB codes are publicly available at https://researchdata.cab.unipd.it/id/eprint/1538 (ref. 57).

References

1. Rinaldo, A., Rigon, R., Banavar, J., Maritan, A. & Rodriguez-Iturbe, I. Evolution and selection of river networks: statistics, dynamics, and complexity. *Proc. Natl Acad. Sci. USA* **111**, 2417–2424 (2014).
2. Busch, M. et al. What's in a name? Patterns, trends, and suggestions for defining non-perennial rivers and streams. *Water* **12**, 1980 (2020).
3. Botter, G. et al. Hierarchical climate-driven dynamics of the active channel length in temporary streams. *Sci. Rep.* **11**, 21503 (2021).
4. Prancevic, J., Seybold, H. & Kirchner, J. Variability of flowing stream network length across the us. *Science* **387**, 782–786 (2025).
5. McDonough, O., Hosen, J. & Palmer, M. in *River Ecosystems: Dynamics, Management and Conservation* (eds Elliot, H. S. & Martin, L. E.) 259–290 (Nova Science, 2011).
6. Stubbington, R., England, J., Wood, P. & Sefton, C. Temporary streams in temperate zones: recognizing, monitoring and restoring transitional aquatic-terrestrial ecosystems. *WIREs Water* **4**, e1223 (2017).
7. Price, A., Jones, C., Hammond, J., Zimmer, M. & Zipper, S. The drying regimes of non-perennial rivers and streams. *Geophys. Res. Lett.* **48**, e2021GL093298 (2021).
8. Godsey, S. & Kirchner, J. Dynamic, discontinuous stream networks: hydrologically driven variations in active drainage density, flowing channels and stream order. *Hydrol. Process.* **28**, 5791–5803 (2014).
9. Hansen, W. Identifying stream types and management implications. *For. Ecol. Manag.* **143**, 39–46 (2001).
10. Wohl, E. The challenges of channel heads. *Earth Sci. Rev.* **185**, 649–64 (2018).
11. Sangireddy, H., Carothers, R., Stark, C. & Passalacqua, P. Controls of climate, topography, vegetation, and lithology on drainage density extracted from high resolution topography data. *J. Hydrol.* **537**, 271–282 (2016).
12. Kim, S., Yoon, S. & Choi, N. Evaluating the drainage density characteristics on climate and drainage area using Lidar data. *Appl. Sci.* **13**, 700 (2023).
13. Melton, M. *An Analysis of the Relations among Elements of Climate, Surface Properties and Geomorphology* (Department of Geology, Columbia University, 1957).
14. Madduma Bandara, C. Drainage density and effective precipitation. *J. Hydrol.* **21**, 187–190 (1974).
15. Abrahams, A. Drainage densities and sediment yields in Eastern Australia. *Austr. Geogr. Stud.* **10**, 19–41 (1972).
16. Daniel, J. Drainage density as an index of climatic geomorphology. *J. Hydrol.* **50**, 147–154 (1981).
17. Moglen, G., Eltahir, E. & Bras, R. On the sensitivity of drainage density to climate change. *Water Resour. Res.* **34**, 855–862 (1998).
18. Gregory, K. in *Geomorphology and Climate* (ed. Derbyshire, E.) 289–315 (Wiley, 1976).
19. Abrahams, A. & Ponczynski, J. Drainage density in relation to precipitation intensity in the U.S.A. *J. Hydrol.* **75**, 383–388 (1984).
20. Stanley, E., Fisher, S. & Grimm, N. Ecosystem expansion and contraction in streams. *BioScience* **47**, 427–435 (1997).
21. Tzoraki, O., Nikolaidis, N., Amaxidis, Y. & Skoulikidis, N. In-stream biogeochemical processes of a temporary river. *Environ. Sci. Technol.* **41**, 1225–1231 (2007).
22. Acuña, V., Hunter, M. & Ruhí, A. Managing temporary streams and rivers as unique rather than second-class ecosystems. *Biol. Conserv.* **211 (Part B)**, 12–19 (2017).
23. Datry, T. et al. A global analysis of terrestrial plant litter dynamics in non-perennial waterways. *Nat. Geosci.* **11**, 497–503 (2018).
24. Stubbington, R. et al. Ecosystem services of temporary streams differ between wet and dry phases in regions with contrasting climates and economies. *People Nat.* **2**, 660–667 (2020).
25. Battin, T. et al. River ecosystem metabolism and carbon biogeochemistry in a changing world. *Nature* **613**, 449–459 (2023).
26. Arthington, A. H., Bernardo, J. & Ilhéu, M. Temporary rivers: linking ecohydrology, ecological quality and reconciliation ecology. *River Res. Apps* **30**, 1209–1215 (2014).
27. Leigh, C. et al. Ecological research and management of intermittent rivers: an historical review and future directions. *Freshwater Biol.* **61**, 1181–1199 (2016).
28. Larned, S., Datry, T., Arscott, D. & Tockner, K. Emerging concepts in temporary-river ecology. *Freshwater Biol.* **55**, 717–738 (2010).
29. Datry, T., Larned, S. & Tockner, K. Intermittent rivers: a challenge for freshwater ecology. *BioScience* **64**, 229–235 (2014).
30. Datry, T. et al. Flow intermittance and ecosystem services in rivers of the anthropocene. *J. Appl. Ecol.* **55**, 353–364 (2018).
31. Costigan, K., Jaeger, K., Goss, C., Fritz, K. & Goebel, P. Understanding controls on flow permanence in intermittent rivers to aid ecological research: integrating meteorology, geology and land cover. *Ecohydrology* **9**, 1141–1153 (2016).
32. Shanafield, M. et al. Science gets up to speed on dry rivers. *Eos* https://doi.org/10.1029/2020EO139902 (2020).
33. Shanafield, M., Bourke, S., Zimmer, M. & Costigan, K. An overview of the hydrology of non-perennial rivers and streams. *WIREs Water* **8**, e1504 (2021).
34. Zipper, S. et al. Pervasive changes in stream intermittency across the United States. *Environ. Res. Lett.* **16**, 084033 (2021).
35. Datry, T. et al. Non-perennial segments in river networks. *Nat. Rev. Earth Environ.* **4**, 815–830 (2023).
36. Acuña, V. et al. Why should we care about temporary waterways? *Science* **343**, 1080–1081 (2014).
37. Brinkerhoff, C., Gleason, C., Kotchen, M., Kysar, D. & Raymond, P. Ephemeral stream water contributions to united states drainage networks. *Science* **384**, 1476–1482 (2024).
38. Messager, M. L. et al. Global prevalence of non-perennial rivers and streams. *Nature* **594**, 391–397 (2021).
39. Gardner, J., Pavelsky, T. & Doyle, M. The abundance, size, and spacing of lakes and reservoirs connected to river networks. *Geophys. Res. Lett.* **46**, 2592–2601 (2019).
40. Lapides, D., Leclerc, C., Moidu, H., Dralle, D. & Hahm, W. Variability of stream extents controlled by flow regime and network hydraulic scaling. *Hydrol. Process.* **35**, e14079 (2021).
41. Bujak-Ozga, I., Von Freyberg, J., Zimmer, M., Rinaldo, A. & Van Meerveld, I. Comparison of the dynamics of the flowing drainage network and water chemistry for four headwater catchments. *Ecohydrology* **18**, e2734 (2024).
42. Wu, H. et al. A new global river network database for macroscale hydrologic modeling. *Water Resour. Res.* **48**, 2012WR012313 (2012).
43. Schneider, A. et al. Global-scale river network extraction based on high-resolution topography and constrained by lithology, climate, slope, and observed drainage density. *Geophys. Res. Lett.* **44**, 2773–2781 (2017).
44. Lehner, B., Verdin, K. & Jarvis, A. New global hydrography derived from spaceborne elevation data. *Eos* **89**, 93–94 (2008).
45. Döll, P. & Lehner, B. Validation of a new global 30-min drainage direction map. *J. Hydrol.* **258**, 214–231 (2002).
46. Linke, S. et al. Global hydro-environmental sub-basin and river reach characteristics at high spatial resolution. *Sci. Data* **6**, 283 (2019).
47. Botter, G. & Durighetto, N. The stream length duration curve: a tool for characterizing the time variability of the flowing stream length. *Water Resour. Res.* **56**, e2020WR027282 (2020).
48. Senatore, A. et al. Monitoring and modeling drainage network contraction and dry down in Mediterranean headwater catchments. *Water Resour. Res.* **57**, e2020WR028741 (2021).

49. Jensen, C. K., McGuire, K., Shao, Y. & Dolloff, C. Modeling wet headwater stream networks across multiple flow conditions in the Appalachian Highlands. *Earth Surf. Process. Landforms* **43**, 2762–2778 (2018).
50. Noto, S., Durighetto, N., Tauro, F., Grimaldi, S. & Botter, G. Characterizing space-time channel network dynamics in a Mediterranean intermittent catchment of central italy combining visual surveys and cameras. *Water Resour. Res.* **60**, e2023WR034682 (2024).
51. Yang, S., Choi, K. & Paik, K. Power law between the apparent drainage density and the pruning area. *Hydrol. Earth Syst. Sci.* **28**, 3119–3132 (2024).
52. Prancevic, J. & Kirchner, J. Topographic controls on the extension and retraction of flowing streams. *Geophys. Res. Lett.* **46**, 2084–2092 (2019).
53. Lin, P., Pan, M., Wood, E., Yamazaki, D. & Allen, G. A new vector-based global river network dataset accounting for variable drainage density. *Sci. Data* **8**, 28 (2021).
54. Maritan, A., Rinaldo, A., Rigon, R., Giacometti, A. & Rodriguez-Iturbe, I. Scaling laws for river networks. *Phys. Rev. E* **53**, 1510–1515 (1996).
55. Beven, K. & Binley, A. The future of distributed model: model calibration and uncertainty prediction. *Hydrol. Process.* **6**, 279–298 (1992).
56. Messager, M. & Lehner, B. Global prevalence of non-perennial rivers and streams. *figshare* https://doi.org/10.6084/m9.figshare.14633022 (2021).
57. Barone, F. & Durighetto, N. *Headwater Streams Control the Non-perennial Fraction of the Global River Network—DATA* (Research Data UNIPD, 2025); https://researchdata.cab.unipd.it/id/eprint/1539
58. Metzger, M. et al. A high-resolution bioclimate map of the world: a unifying framework for global biodiversity research and monitoring. *Global Ecol. Biogeogr.* **22**, 630–638 (2013).
59. lehner, B. & Grill, G. Global river hydrography and network routing: baseline data and new approaches to study the world's large river systems. *Hydrol. Process.* **27**, 2171–2186 (2013).

Acknowledgements

We thank S. Basso for insightful comments on this paper.
The research was carried out in the context of the ERC project 'DyNET' (H2020 European Research Council, grant no. 770999, G.B.).

Author contributions

G.B. and N.D. conceived and designed research; F.B., N.D. and G.B. performed research; G.B., F.B. and N.D. analysed and discussed results; F.B. prepared all figures; G.B. wrote the paper with important contributions from all authors.

Competing interests

The authors declare no competing interests.

Additional information

Supplementary information The online version contains supplementary material available at https://doi.org/10.1038/s44221-025-00549-x.

Correspondence and requests for materials should be addressed to Gianluca Botter.

Peer review information *Nature Water* thanks Mathis Messager and the other, anonymous, reviewer(s) for their contribution to the peer review of this work.